

# Dependence of the Current and Power Efficiencies of Organic Light-Emitting Diode on the Thickness of the Constituent Organic Layers

Chengfeng Qiu, Haiying Chen, Man Wong, *Senior Member, IEEE*, and Hoi S. Kwok, *Senior Member, IEEE*

**Abstract**—The dependence of the current and power efficiencies of bi-layer organic light-emitting diodes (OLEDs) on the thickness of the constituent organic layers is reported. The thickness of the electron and hole transport layers was simultaneously varied to determine the optimal configuration for power efficiency. It was verified that the inclusion of a suitable electrode buffer layer reduced the effective energy barrier against carrier injection, thus improved the injection efficiency. An optimal thickness for the electrode buffer layer was also identified and explained.

**Index Terms**—Alq<sub>3</sub>, CuPc, electrode buffer layer, organic light-emitting diode, TPD.

## I. INTRODUCTION

**T**HOUGH liquid-crystal display is presently the dominant flat-panel display technology because of its portability, low power consumption, and mature manufacturing practice, organic light-emitting diode (OLED) has attracted great attention [1]–[3] since the demonstration of efficient electro-luminescence (EL) from a bi-layer device by Tang *et al.* [4]. In addition to sharing many of the favorable attributes with liquid-crystals, OLEDs are attractive as alternative display components because of their relative merits of being self-emitting, having large intrinsic viewing angle and fast switching speed. However, because of their relatively short history of development, much remains to be explored in terms of their basic device physics and design, manufacturing techniques, stability, and integration with such active electronic elements as transistors [5]–[8].

Efficient EL in an organic semiconductor requires not only balanced injection of but also similar mobility values for electrons and holes. This is accomplished in a bi-layer OLED by incorporating an electron transport layer (ETL), in which conduction is dominated by electrons, and a separate hole transport layer (HTL), in which conduction is dominated by holes. This configuration allows independent optimization of the injection and transport characteristics using, respectively, properly selected electrodes and transport materials. The energy levels of the ETL and the HTL are designed to give rise to an energy barrier that confines the radiative decay of electron-hole pairs

(excitons) to within an emission zone close to the ETL/HTL interface and away from the conducting electrodes, thus reducing image-charge-induced radiation quenching due to interference effects.

For a large class of organic semiconductors, conduction at low to medium current density is limited by thermionic emission of the dominant charge carriers over the energy barrier at the interface between the emitting electrode and the corresponding transport layer [9]. A higher energy barrier gives rise to a larger impediment against carrier injection, thus resulting in increased diode “turn-on” voltage and reduced luminous flux power efficiency ( $\eta$ )—defined as the ratio of the luminous flux output of the EL device to the corresponding driving electrical power. For a given material combination of ETL and HTL, it has been found that the injection efficiency can be improved by inserting a buffer layer between the electrode and the transport layer [10]—if the buffer layer is appropriately chosen so that its energy level is intermediate between the Fermi level of the electrode and the corresponding energy level of the dominant charge carriers of the transport layer.

Though further improvement in luminous efficiency using a variety of other techniques has been reported, such as the use of multi- [11], [12] or mixed [13], [14] transport layers and the incorporation of emission/recombination dopants [15], [16], little has been reported on the dependence of  $\eta$  and the luminance current efficiency ( $\gamma$ )—defined as the ratio of the output luminance ( $L$ ) to the driving current density ( $J$ )—on the thickness of the ETL, HTL, and the electrode buffer layer of OLEDs with a given material combination.

The two efficiencies  $\eta$  and  $\gamma$  are not independent. Assuming a Lambertian emission pattern [17]

$$\eta = \frac{\pi L}{VJ} = \pi \frac{1}{V} \left( \frac{L}{J} \right) \equiv \pi \frac{\gamma}{V} \quad (1)$$

where  $L$  is measured normal to the emitting surface and  $V$  is the applied voltage. While  $\gamma$  depends on the optical coupling and the internal quantum efficiencies [18], it is fairly constant or only weakly varying over a large range of  $J$ . On the other hand,  $\eta$  is clearly bias dependent and inversely proportional to  $V$ . Typical examples of the dependence of  $\eta$  and  $\gamma$  on  $J$  are shown in Fig. 1. Note how  $\eta$  peaks at a low bias and decreases monotonically with increasing  $J$ .

In this paper, detailed study has been performed on OLEDs based on tris-8-hydroxyquinoline aluminum (Alq<sub>3</sub>) as the ETL and the principal emission layer, N, N'-diphenyl-N, N'

Manuscript received December 27, 2000; revised May 14, 2001. This work was supported by a grant from the Research Grants Council of the Hong Kong Special Administrative Region. This review of this paper was arranged by Editor J. Hynccek.

The authors are with the Center for Display Research, Department of Electrical and Electronic Engineering, the Hong Kong University of Science and Technology, Clear Water Bay, Kowloon, Hong Kong (e-mail: eem-wong@ee.ust.hk).

Publisher Item Identifier S 0018-9383(01)07324-5.

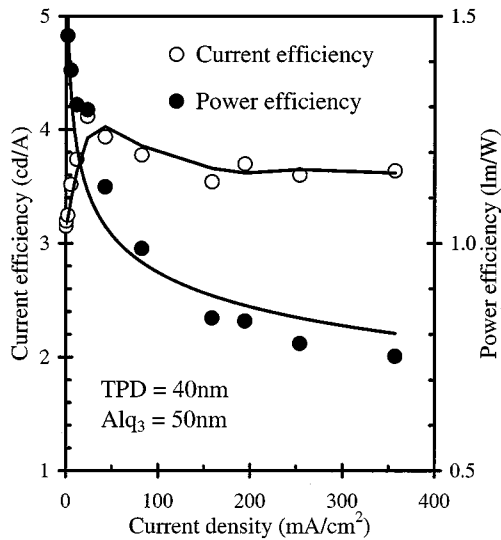


Fig. 1. Dependence of the current and power efficiencies on driving current density.

bis (3-methylphenyl)-1, 1'-biphenyl-4, 4'-diamine (TPD) as the HTL and copper phthalocyanine (CuPc) as the electrode (anode) buffer layer. The OLEDs were characterized in terms of their  $\eta$  and  $\gamma$ . The optimal thickness for the various constituent organic layers has been identified and discussed.

## II. OLED FABRICATION

Glass coated with 75-nm thick indium-tin oxide (ITO) was used as the starting substrate. The sequence of pre-cleaning prior to loading into the evaporation chamber consisted of soaking in ultra-sonic detergent for 30 min, spraying with de-ionized (DI) water for 10 min, soaking in ultrasonic DI water for 30 min, oven bake-dry for 1–2 h, and ITO surface stabilizing ultraviolet ozone illumination [19] for 9 min.

The base pressure in the evaporator was about 8  $\mu$ Torr. The constituent organic thin films were deposited from sublimation of commercial grade Alq<sub>3</sub>, TPD and CuPc powder loaded in resistively heated evaporation cells. The deposition rates of the organic thin films were 0.2–0.4 nm/s. While the ITO formed the anodes of the OLEDs, composite layers of 1 nm lithium fluoride (LiF) topped with 150 nm aluminum (Al) were used as the cathodes [20]. The deposition rates of LiF and Al were 0.02–0.05 nm/s and 1–1.5 nm/s, respectively. Film thickness was determined *in situ* using a crystal monitor.

The basic OLED structure (Fig. 2) studied consisted of ITO/CuPc/TPD/Alq<sub>3</sub>/LiF/Al, with the CuPc anode buffer layer (ABL) optionally removed. Diodes with 5% rubrene doping in the TPD layers and exhibiting higher emission efficiencies were also separately studied. A set of shadow masks was used to define the 4-mm diameter OLEDs. The devices were characterized in room ambient and temperature without encapsulation. EL photometric characteristics were measured using a Kollmorgen Instrument PR650 photo-spectrometer. Current–voltage ( $I$ – $V$ ) characteristics were measured using a Hewlett-Packard HP4145B Semiconductor Parameter Analyzer.

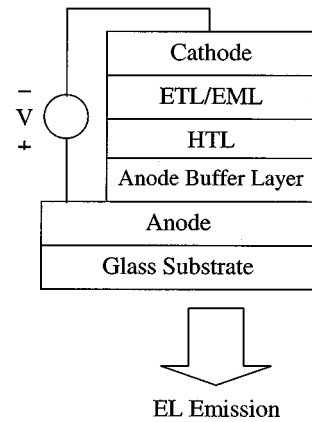


Fig. 2. Bi-layer OLED basic structure.

TABLE I  
THICKNESS OF Alq<sub>3</sub> AND TPD INVESTIGATED

ITO/CuPc (20nm)/TPD/Alq <sub>3</sub> /LiF (1.0nm)/Al (150nm)							
TPD (nm)	Alq <sub>3</sub> (nm)	TPD (nm)	Alq <sub>3</sub> (nm)	TPD (nm)	Alq <sub>3</sub> (nm)	TPD (nm)	Alq <sub>3</sub> (nm)
20	30	30	30	40	30	50	30
	40		40		40		
	50		50		50		
	60		60		60		

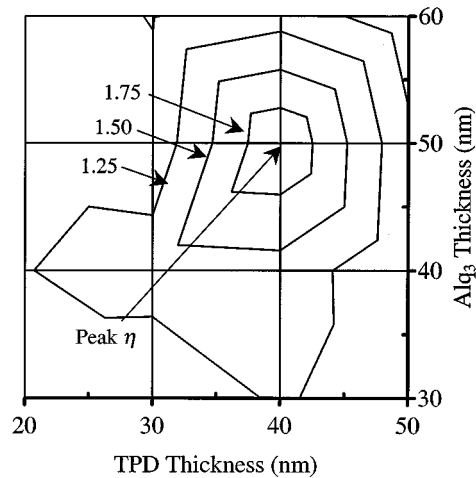


Fig. 3. Contour plot of the luminous flux power efficiencies ( $\eta$ ) of OLEDs with different Alq<sub>3</sub> and TPD thickness values. The TPD is not doped with rubrene and the numbers labeling the contours are values of  $\eta$  in lm/W.

## III. EFFECTS OF Alq<sub>3</sub> AND TPD THICKNESS

The thickness combinations of Alq<sub>3</sub> and TPD investigated are summarized in Table I. The thickness of Alq<sub>3</sub> and TPD was varied from 30 nm to 60 nm and from 20 nm to 50 nm, respectively. At an increment of 10 nm, a complete permutation of 16 configurations was studied. The TPD layers in these devices were not doped with rubrene and 20-nm CuPc ABLs were used in all of the OLEDs.

Shown in Fig. 3 is a contour plot of the peak  $\eta$  of OLEDs with different Alq<sub>3</sub> and TPD thickness, where  $\eta$  is calculated according to (1) using  $L$  measured along the normal to the emitting surface. An optimal  $\eta$  clearly exists within the range of thickness explored, with a maximum value of  $\sim$ 2 lm/W measured for the device with 40 nm TPD and 50 nm Alq<sub>3</sub>. As a comparison, a maximum  $\eta$  of 5 lm/W was measured in devices with

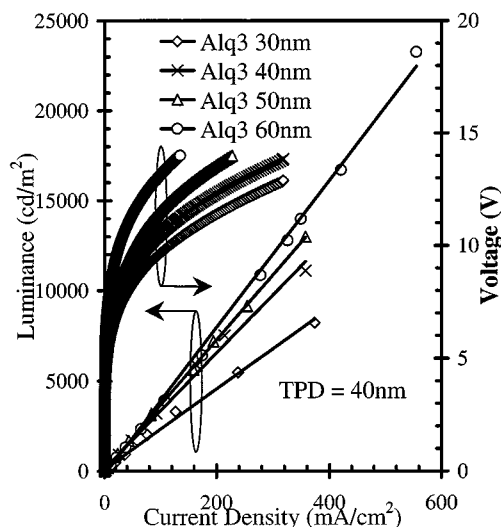


Fig. 4. Dependence of OLED Luminance ( $L$ )—current density ( $J$ )—voltage ( $V$ ) characteristics on the thickness of Alq<sub>3</sub>. The thickness of TPD is fixed at 40 nm.

rubrene-doped TPD. The behavior shown in Fig. 3 further indicates that when the thickness of either the TPD or the Alq<sub>3</sub> is fixed,  $\eta$  invariably exhibits a maximum as that of the other is systematically varied. Two such typical series are reported, one collected from OLEDs with a fixed TPD thickness and the other from OLEDs with a fixed Alq<sub>3</sub> thickness.

For the series with a fixed TPD thickness, the device structure studied was ITO/CuPc (20 nm)/TPD (40 nm)/Alq<sub>3</sub>/LiF (1 nm)/Al (150 nm). The thickness of Alq<sub>3</sub> was varied from 30 nm to 60 nm. Shown in Fig. 4 are the corresponding “Luminance ( $L$ )—current density ( $J$ )—voltage ( $V$ )” characteristics. Independent of the Alq<sub>3</sub> thickness,  $L$  was found to increase linearly with  $J$ . Therefore, it is possible to calculate the luminance current efficiency ( $\gamma$ ) as the ratio of  $L$  to  $J$ . The dependence of the relative luminance current efficiency (Rel- $\gamma$ ), the relative luminous flux power efficiency (Rel- $\eta$ ) and the turn-on voltage ( $V_{on}$ ) on Alq<sub>3</sub> thickness is shown in Fig. 5. The two relative efficiencies are defined as the ratios of  $\gamma$  and  $\eta$  at a given Alq<sub>3</sub> thickness to the respective maximum values for the series.  $V_{on}$  is defined as the smallest voltage at which luminescence is visually detected. For any given  $J$ , Rel- $\gamma$  increases with increasing Alq<sub>3</sub> thickness. This is expected since the separation between the exciton recombination zone, which is confined to a region of about 20 nm from the TPD/Alq<sub>3</sub> interface [21], and the cathode electrode increases with increasing Alq<sub>3</sub> thickness. Consequently, image dipole-induced radiation quenching is reduced.

However, the observed monotonic increase in  $\gamma$  within the range of Alq<sub>3</sub> thickness studied does not lead to a similar behavior in  $\eta$ . It can be seen from the  $V$ – $J$  characteristics (Fig. 4) that  $V_{on}$  increases monotonically with increasing Alq<sub>3</sub> thickness. This is not surprising since the electric field at a given  $V$  progressively decreases with increasing thickness, thus adversely affecting both the injection and the transport of charge carriers. Consequently,  $\eta$  first increases with increasing Alq<sub>3</sub> thickness due to improved  $\gamma$  then decreases with further increase in thickness due to increase in  $V_{on}$ . The highest  $\eta$  is obtained at an Alq<sub>3</sub> thickness of 50 nm, as shown in Fig. 5.

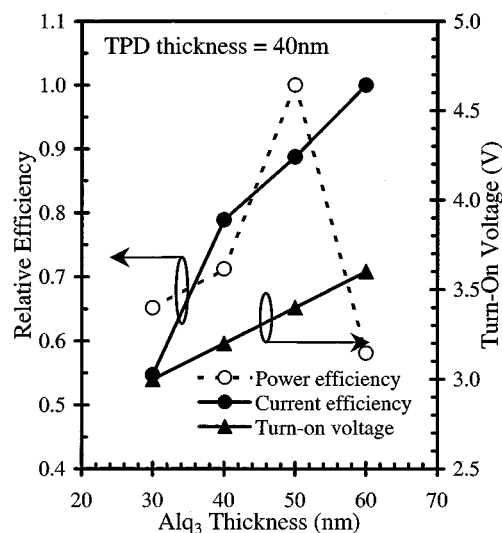


Fig. 5. Dependence of the relative luminance current efficiency, luminous flux power efficiency and the turn-on voltage on the thickness of Alq<sub>3</sub>.

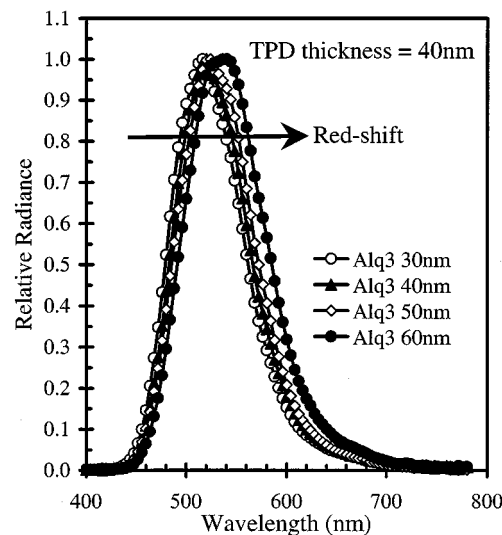


Fig. 6. Dependence of the EL spectra on the thickness of Alq<sub>3</sub>. The radiance values have been normalized by the peak radiance of each spectrum.

The EL spectra taken along the direction of the surface normal of the OLEDs with different Alq<sub>3</sub> thickness are shown in Fig. 6. The characteristic spectral attributes are summarized in Table II. While the full widths at half maximum (FWHM) of 84 nm to 96 nm are relatively constant as the Alq<sub>3</sub> thickness is increased by 30 nm from 30 nm to 60 nm, there is a  $\sim$ 24 nm red-shift of the spectral peak. This shift has been associated with the dependence of the micro-cavity-induced wave-guiding effects on Alq<sub>3</sub> thickness [18]. The ratio of the shift to the change in Alq<sub>3</sub> thickness is  $\sim$ 0.8, which is close to the value of  $\sim$ 0.7 reported for the roughly similar OLED configurations [18] with 4, 4'-bis[N-(1-naphthyl)-N-phenylamino] biphenyl ( $\alpha$ -NPD) as the HTL.

For the series with a fixed Alq<sub>3</sub> thickness, the device structure studied was ITO/CuPc (20 nm)/TPD/Alq<sub>3</sub> (50 nm)/LiF (1 nm)/Al (150 nm). The thickness of TPD was varied from 30 nm to 70 nm. The corresponding  $L$ – $J$ – $V$  characteristics are shown in Fig. 7. Again,  $L$  is found to increase linearly with increasing  $J$

TABLE II  
EL SPECTRA CHARACTERISTICS AT DIFFERENT Al<sub>3</sub> THICKNESS VALUES

OLED Structure: ITO/CuPc (20nm)/TPD (40nm)/Alq <sub>3</sub> /LiF (1.0nm)/Al (150nm)				
Al <sub>3</sub> Thickness	30nm	40nm	50nm	60nm
Peak	516nm	520nm	524nm	540nm
WLHM (FWHM)	479, 562nm (83nm)	483, 566nm (83nm)	485, 572nm (87nm)	491, 585nm (94nm)

WLHM-Wavelength at half maximum, FWHM-Full width at half maximum

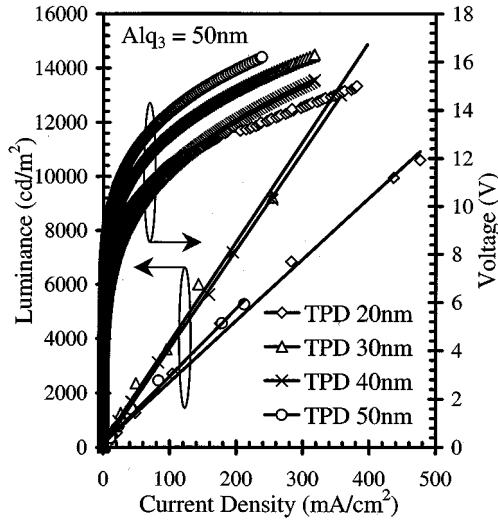


Fig. 7. Dependence of the  $L$ - $J$ - $V$  characteristics on the thickness of TPD. The thickness of Al<sub>3</sub> is fixed at 50 nm.

for all TPD thickness. The relative efficiencies, Rel- $\gamma$  and Rel- $\eta$ , are similarly defined as the ratios of  $\gamma$  and  $\eta$  at a given TPD thickness to the respective peak values of the series. Unlike the case for the Al<sub>3</sub> series, Rel- $\gamma$  only increases as the TPD thickness is increased from 30 nm to 40 nm but decreases with further increase in TPD thickness (Fig. 8). A plausible reason for the initial increase in  $\gamma$  could be reduced radiation quenching as the recombination zone is moved further away from the ITO electrode, but the reason for the subsequent decrease of  $\gamma$  with TPD thickness is presently not clear.

The trend for Rel- $\eta$  tracks closely that for Rel- $\gamma$ . From the  $V$ - $J$  characteristics (Fig. 7), it can be seen that  $V_{on}$  shows the expected monotonic increase (Fig. 8) with increasing TPD thickness. Consequently,  $\eta$  first increases with increasing TPD thickness from 30 nm to 40 nm because of improved  $\gamma$ , then decreases with further increase in thickness because of both increase in  $V_{on}$  and decrease in  $\gamma$ . The highest  $\eta$  is obtained at a TPD thickness of 40 nm.

The corresponding EL spectra for the OLEDs with different TPD thickness are shown in Fig. 9. Interestingly, while the locations of the EL peaks are relatively independent of the TPD thickness, there is a clear red-shift in the right halves (longer wavelength) of the spectra. Though the red-shift is still consistent with the thickness dependence of micro-cavity waveguiding effects, it is not clear why the change in the spectral shape with TPD thickness is not the same as that associated with the fixed-TPD series shown in Fig. 6. The EL spectral characteristics of this series of OLEDs are summarized in Table III.

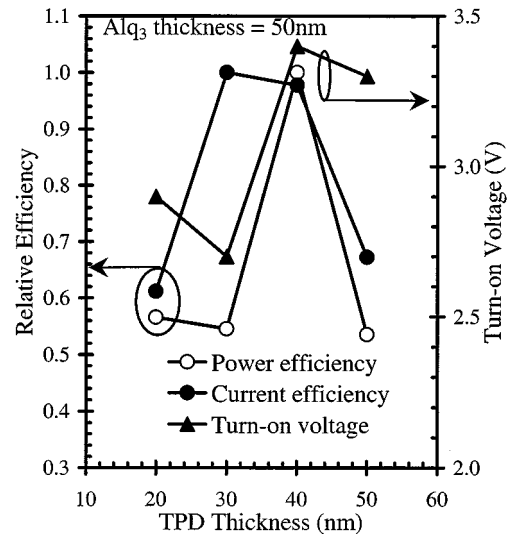


Fig. 8. Dependence of the relative luminance current efficiency, luminous flux power efficiency and the turn-on voltage on the thickness of TPD.

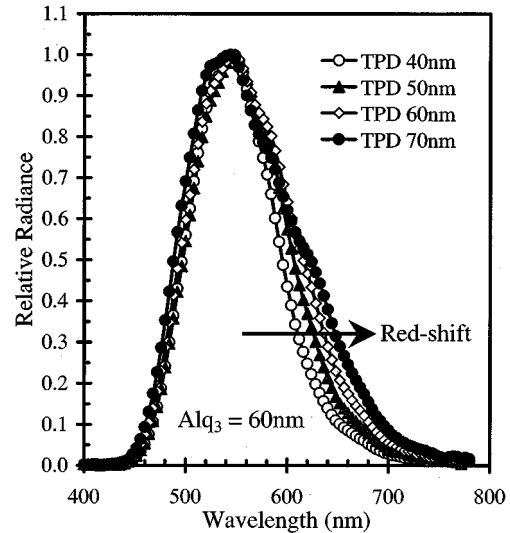


Fig. 9. Dependence of the EL spectrum on the thickness of TPD. The radiance values have been normalized by the peak radiance of each spectrum.

TABLE III  
EL SPECTRA CHARACTERISTICS AT DIFFERENT TPD THICKNESS VALUES

OLED Structure: ITO/CuPc (20nm)/TPD/Alq <sub>3</sub> (50nm)/LiF (1.0nm)/Al (150nm)				
TPD Thickness	40nm	50nm	60nm	70nm
Peak	540nm	548nm	548nm	548nm
WLHM	496, 595nm	497, 606nm	493, 616nm	488, 623nm
FWHM	(99nm)	(109nm)	(123nm)	(135nm)

WLHM-Wavelength at half maximum, FWHM-Full width at half maximum

#### IV. EFFECTS OF ELECTRODE BUFFER LAYER

The effects of ABL have been studied using an OLED structure of ITO/CuPc/TPD (40 nm)/Alq<sub>3</sub> (50 nm)/Ag. Silver was used as the cathode electrode, instead of the more efficient composite LiF/Al. The thickness of CuPc was varied from 0 nm to 25 nm. The corresponding  $L$ - $J$ - $V$  characteristics are shown in Fig. 10. It can be seen that the  $L$ - $J$  curves largely overlap, indicating  $\gamma$  is relatively independent of CuPc thickness. This independence is not consistent with the result that  $\gamma$  is dependent

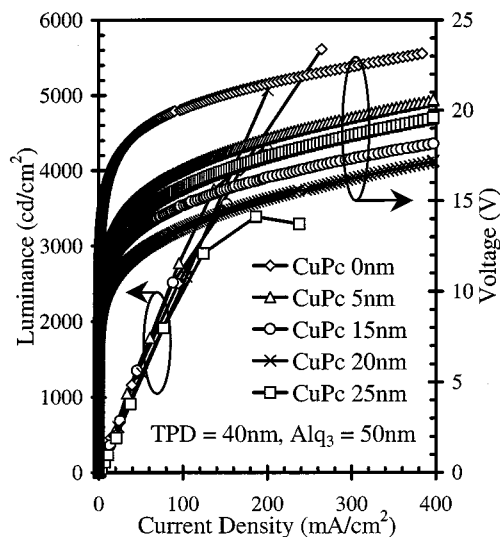


Fig. 10. Dependence of the  $L$ - $J$ - $V$  characteristics on the thickness of CuPc. The thickness values of TPD and Alq<sub>3</sub> are fixed at 40 and 50 nm, respectively.

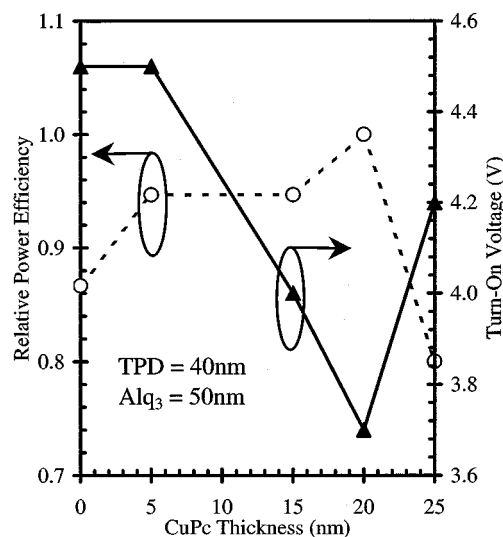


Fig. 12. Dependence of the relative luminance current efficiency and the turn-on voltage on the thickness of CuPc.

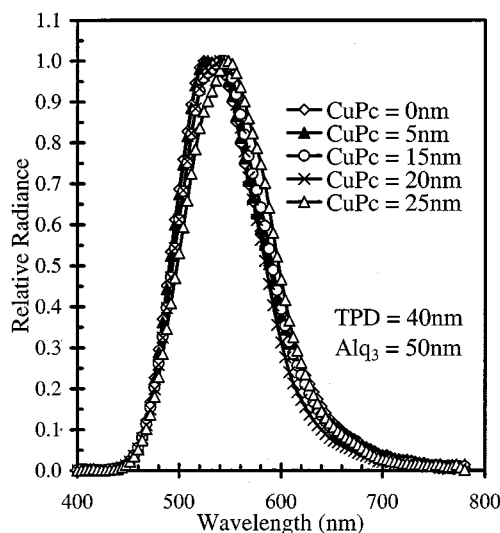


Fig. 11. Dependence of the EL spectrum on the thickness of CuPc. The radiance values have been normalized by the peak radiance of each spectrum.

on HTL thickness (Fig. 8), given that CuPc is just an additional organic layer inserted between the anode and the HTL.

The corresponding EL spectra are shown in Fig. 11. While the FWHM are relatively constant with increasing CuPc thickness, there is a red-shift in the spectral peak by  $\sim 24$  nm, similar to the behavior of the series with the fixed TPD thickness (Fig. 6). The behavior of the  $V$ - $J$  characteristics is rather more interesting. Instead of increasing monotonically with thickness as in the cases of Alq<sub>3</sub> and TPD,  $V_{on}$  first decreases with increasing CuPc thickness, reaches a minimum at about 20 nm, then increases as the CuPc thickness is further increased.

The initial reduction in  $V_{on}$  (Fig. 12) is caused by a decrease in the effective hole injection barrier. This is fundamentally linked to the highest-occupied molecular orbital (HOMO) level of CuPc being situated between that of the TPD and the Fermi level of the ITO anode. Because of the separation between the ITO/CuPc injection interface and the CuPc/TPD interface, the HOMO levels of CuPc and TPD at the CuPc/TPD interface can

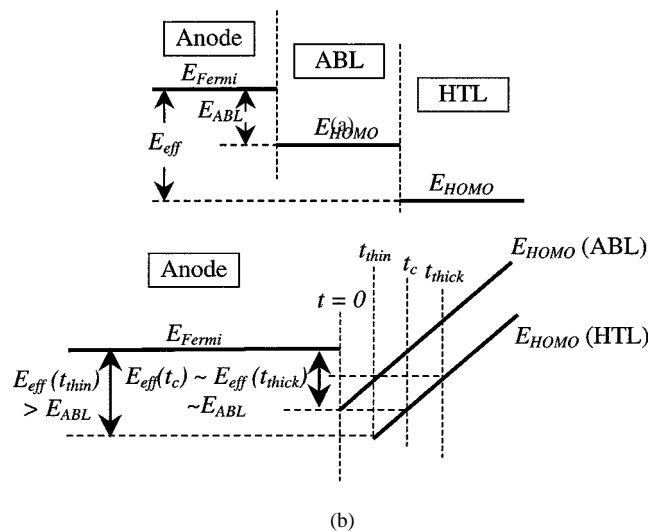


Fig. 13. Schematic diagram of the energy levels of the ABL and HTL (a) without and (b) with an applied anode electric field.

be modulated by the internal electric field. This modulation is responsible for the reduction in the effective hole injection barrier [22].

The situation can be better understood by studying the energy level diagrams in Fig. 13. The zero-field energy level diagram is shown in Fig. 13(a). The effective injection barrier ( $E_{eff}$ ) is simply the difference between the Fermi level of the anode and the HOMO level of the HTL. The presence of the ABL does not affect this effective barrier height. With the application of an electric field ( $F_a$ ), slopes are induced in the HOMO levels of the ABL and the HTL. Disregarding image-force lowering effects and ignoring the difference between the dielectric constants, the new energy level diagram is schematically shown in Fig. 13(b) for three different ABL thickness values:  $t_{thin}$ ,  $t_c$ , and  $t_{thick}$ .  $E_{eff}$  is still measured by the difference between the Fermi level of the anode and the field-modulated HOMO level of the HTL. When the thickness ( $t$ ) of the ABL is "small" (i.e.,  $t \sim t_{thin}$ ), there is some reduction in  $E_{eff}$ , but it is still larger

than the barrier ( $E_{\text{ABL}}$ ) at the anode/ABL interface. When a critical ABL thickness ( $t_c$ ) is reached,  $E_{\text{eff}}$  is exactly the same as  $E_{\text{ABL}}$ . Consequently, the effective hole injection barrier decreases monotonically with increasing ABL thickness from 0 to  $t_c$ . Additional reduction in  $E_{\text{eff}}$  by further increasing the ABL thickness beyond  $t_c$  is no longer productive because of the relatively weak modulation, by image-force lowering, of the  $E_{\text{ABL}}$  barrier. In fact, any additional ABL thickness beyond  $t_c$  contributes more to conduction loss and causes an increase, instead of a further reduction, in  $V_{\text{on}}$ . Indeed, this is observed in Fig. 12 when the CuPc thickness is increased from 20 nm to 25 nm.

For a given  $F_a$ ,  $t_c$  should be just large enough to eliminate the barrier presented by the difference ( $\Delta E$ ) between the HOMO levels of the HTL and the ABL. Because of conduction loss,  $F_a$  is not a constant inside the ABL. However, one can roughly estimate  $t_c$  by assuming a constant  $F_a$  throughout the buffer layer

$$t_c \approx \frac{\Delta E}{qF_a} \quad (2)$$

where  $q$  is the fundamental electronic charge. This implies  $t_c$  should increase with  $\Delta E$  and decrease with  $F_a$ . For the CuPc and TPD system,  $\Delta E$  is about  $\sim 1.0$  eV. Therefore  $t_c$  is  $\sim 10$  nm at an  $F_a$  of 1 MV/cm. This qualitative estimate is not too different from the experimentally determined optimal thickness of 20 nm.

## V. CONCLUSION

OLEDs based on the structure of ITO/CuPc/TPD/Alq<sub>3</sub>/LiF/Al has been systematically studied. For all three Alq<sub>3</sub>, TPD, and CuPc layers, excessively thick films lead to high turn-on voltage, thus degrade the luminous flux power efficiency. For Alq<sub>3</sub> and TPD, excessively thin films lead to reduction in luminance current efficiency. Finally, excessively thin CuPc reduces the effectiveness of hole injection barrier modulation, thus degrades the overall power efficiency. For optimal power efficiency, the thickness of Alq<sub>3</sub>, TPD, and CuPc are 50 nm, 40 nm, and 20 nm, respectively. At this optimal configuration, a luminance of 24 000 cd/m<sup>2</sup> is obtained at a current density of 560 mA/cm<sup>2</sup>. The respective luminous flux power efficiencies are  $\sim 2$  lm/W or  $\sim 5$  lm/W, with or without the 5% rubrene dopant in TPD. These values are comparable to those reported in the research literature.

## REFERENCES

- [1] P. E. Burrows, G. Gu, V. Bulovic, Z. Shen, S. R. Forrest, and M. E. Thompson, "Achieving full-color lightweight, flat-panel displays," *IEEE Trans. Electron Device*, vol. 44, pp. 1188–1202, Aug. 1997.
- [2] Y. Kijima, N. Asai, and S. Tamura, "A Blue organic light emitting diode," *Jpn. J. Appl. Phys.*, vol. 38, pp. 5274–5277, 1999.
- [3] R. H. Jordan, A. Dodabalapur, M. Strukelj, and T. M. Miller, "White organic electroluminescence devices," *Appl. Phys. Lett.*, vol. 68, no. 9, pp. 1192–1194, 1996.
- [4] C. W. Tang and S. A. Van Slyke, "Organic electroluminescent diode," *Appl. Phys. Lett.*, vol. 51, pp. 913–915, 1987.
- [5] V.-E. Choong, S. Shi, and J. Curless, "Bipolar transport organic light emitting diodes with enhanced reliability by LiF doping," *Appl. Phys. Lett.*, vol. 76, pp. 958–960, 2000.

- [6] H. Kojima, A. Ozawa, T. Takahashi, M. Nagaka, T. Homma, T. Nagatomo, and O. Omoto, "A structural study for highly efficient electroluminescence cells using perylene-doped organic materials," *J. Electrochem. Soc.*, vol. 144, no. 10, pp. 3628–3633, 1997.
- [7] P. F. Tian, V. Bulovic, P. E. Burrows, G. Gu, and S. R. Forrest, "Precise, scalable shadow mask patterning of vacuum-deposited organic light emitting devices," *J. Vac. Sci. Technol.*, vol. A17, no. 5, pp. 2975–2981, 1999.
- [8] Z. Meng, H. Chen, C. Qiu, H. S. Kwok, and M. Wong, "Application of metal-induced unilaterally crystallized polycrystalline silicon thin-film transistor technology to active-matrix organic light-emitting diode," in *IEDM Tech. Dig.*, Dec. 2000, pp. 611–614.
- [9] U. Wolf, V. I. Arkhipov, and H. Bassler, "Current injection from a metal to a disordered hopping system, I: Monte Carlo simulation," *Phys. Rev. B, Condens. Matter*, vol. 59, no. 11, pp. 7507–7513, 1999.
- [10] S. A. Van Slyke, C. H. Chen, and C. W. Tang, "Organic electroluminescent devices with improved stability," *Appl. Phys. Lett.*, vol. 69, no. 15, pp. 2160–2162, 1996.
- [11] H. An, B. Chen, J. Hou, J. Shon, and S. Lin, "Exciton confinement in organic multiple quantum well structures," *J. Phys. D, Appl. Phys.*, vol. 31, pp. 1144–1148, 1998.
- [12] T. Mori, K. Obata, K. Imaizumi, and T. Mizutani, "Preparation and properties of an organic light emitting diode with two emission colors dependent on the voltage polarity," *Appl. Phys. Lett.*, vol. 69, no. 22, pp. 3309–3310, 1996.
- [13] V.-E. Choong, S. Shi, J. Curless, C.-C. Shieh, H.-C. Lee, and F. So, "Organic light-emitting diodes with a bipolar transport layer," *Appl. Phys. Lett.*, vol. 75, no. 2, pp. 172–174, 1999.
- [14] Z. D. Popovic, H. Aziz, C. P. Tripp, N.-X. Hu, A.-M. Hor, and G. Xu, "Improving the efficiency and stability of organic light emitting devices using mixed emitting layer," *Proc. SPIE*, vol. 3476, pp. 68–73, 1998.
- [15] J. Shi and C. W. Tang, "Doped organic electroluminescent devices with improved stability," *Appl. Phys. Lett.*, vol. 70, no. 13, pp. 1665–1667, 1997.
- [16] A. Yamamori, C. Adachi, T. Koyama, and Y. Taniguchi, "Doped organic light emitting diodes having a 650-nm-thick hole transport layer," *Appl. Phys. Lett.*, vol. 72, pp. 2147–2149, 1998.
- [17] J.-S. Kim, P. K. H. Ho, N. C. Greenham, and R. H. Friend, "Electroluminescence emission pattern of organic light-emitting diodes implications for device efficiency calculations," *J. Appl. Phys.*, vol. 88, no. 2, pp. 1073–1081, 2000.
- [18] V. Bulovic, V. B. Khalfin, G. Gu, P. E. Burrows, D. Z. Garbuzov, and S. R. Forrest, "Weak microcavity effects in organic light-emitting devices," *Phys. Rev. B, Condens. Matter*, vol. 58, no. 7, pp. 3730–3740, 1998.
- [19] H.-N. Lin, S.-H. Chen, G.-Y. Perng, and S.-A. Chen, "Nanoscale surface electrical properties of indium-tin-oxide films for organic light emitting diodes investigated by conducting atomic force microscopy," *J. Appl. Phys.*, vol. 89, no. 7, pp. 3976–3979, 2001.
- [20] M. Matsumura, A. Ito, and Y. Miyamae, "Accumulation of positive charges in organic light-emitting diode with a double-layer structure," *Appl. Phys. Lett.*, vol. 75, no. 8, pp. 1042–1044, 1999.
- [21] C. W. Tang, S. A. VanSlyke, and C. H. Chen, "Electroluminescence of doped organic thin films," *J. Appl. Phys.*, vol. 65, no. 9, pp. 3610–3616, 1989.
- [22] V. I. Arkhipov and H. Bassler, "Tandem injection of charge carriers across a metal-dielectric interface," *Appl. Phys. Lett.*, vol. 77, no. 17, pp. 2758–2760, 2000.

**Chengfeng Qiu** received the B.S. degree in physics from Nankai University, Tianjin, China, in 1982, and the Ph.D. degree in material science from Xian Jiaotong University, Xian, China, in 1993.

From 1982 to 1993, he was with the Electronic Engineering Department, Xian Jiaotong University, conducting research on the modification of material surfaces using ion beam treatment, ion implantation, and thin-film deposition. From 1993 to 1995, he was with Tianma Microelectronics, China, where he worked on liquid-crystal displays. From 1995 to 2000, he was with STD, China, and was the Vice-President responsible for the research, development, and manufacturing of liquid-crystal display products. Currently, he is a Postdoctoral Fellow at the Center for Display Research at the Hong Kong University of Science and Technology, Hong Kong, conducting research on organic light-emitting diodes.

**Haiying Chen** received the B.Eng. and M.Eng. degrees in material science and engineering from Tsinghua University, Beijing, China, in 1996 and 1999, respectively. She is currently pursuing the Ph.D. degree in the Department of Electrical and Electronic Engineering at the Hong Kong University of Science and Technology, Hong Kong.

**Man Wong** (S'83–M'84–SM'00) was born in Beijing, China. He received the B.S. and M.S. degrees in electrical engineering from the Massachusetts Institute of Technology, Cambridge, in 1984. From 1985 to 1988, he was at the Center for Integrated Systems at Stanford University, Stanford, CA, where he worked on tungsten gate MOS technology and received the Ph.D. degree, also in electrical engineering, in 1988.

He then joined the Semiconductor Process and Design Center of Texas Instruments, where he worked on the modeling and development of IC metallization systems and dry/vapor cleaning processes. In 1992, he joined the faculty of the Department of Electrical and Electronic Engineering at the Hong Kong University of Science and Technology, Hong Kong. His current research interests include microfabrication technology, device structures and materials, thin-film transistors, organic light-emitting diodes, display technologies, and integrated micro-systems.

Dr. Wong is a member of Tau Beta Pi, Eta Kappa Nu, and Sigma Xi.

**Hoi Sing Kwok** (S'73–M'78–SM'84) received the Ph.D. degree in applied physics from Harvard University, Cambridge, MA, in 1978.

He joined the State University of New York at Buffalo in 1980 as an Assistant Professor in the Department of Electrical and Computer Engineering, and was promoted to Full Professor in 1985. He joined the Hong Kong University of Science and Technology, Hong Kong, in December 1992, and is currently Director of the Center for Display Research. He has over 250 refereed publications and holds over ten patents in optics and LCD technologies.

Dr. Kwok was awarded the U.S. Presidential Young Investigator Award in 1984 and is a Fellow of the Optical Society of America. He is currently Chairman of the Society of Information Display Hong Kong Chapter.